Mass balance of free tropospheric aerosol at the Puy de Dôme (France) in winter

Karine Sellegri, P Laj, F Peron, R Dupuy, Michel E Legrand, Suzanne Preunkert, Jean-Philippe Putaud, Hélène Cachier, Grazia Ghermandi

Mass balance of free tropospheric aerosol at the Puy de Dôme (France) in winter

K. Sellegri,[1] P. Laj,[1] F. Peron,[1] R. Dupuy,[1] M. Legrand,[2] S. Preunkert,[2] J.-P. Putaud,[3] H. Cachier,[4] and G. Ghermandi[5]

Received 11 July 2002; revised 12 December 2002; accepted 20 February 2003; published 5 June 2003.

[1] The size-segregated chemical composition of aerosols was investigated during winters 2000 and 2001 at Puy de Dôme (1465 m above sea level, France), a site most of the time located in the free troposphere. Aerosols have been sampled using low-pressure cascade impactors (Electrical Low Pressure Impactor (ELPI) and Small Deposition Impactor (SDI) 13 and 12 stages) and analyzed for inorganic (Na^+, NH_4^+, K^+, Mg^{2+}, Ca^{2+}, Cl^-, NO_3^-, and SO_4^{2-}) and organic ($HCOO^-$, CH_3COO^-, and $C_2O_4^{2-}$) ions, organic and elemental carbon (OC and EC), insoluble dust, and total mass. Under cloudy conditions, the sampling includes interstitial aerosol as well as the residue of evaporated cloud droplets. Aerosols (and residues of cloud droplets) were sampled in different air masses, which can be classified into three different categories according to their aerosol load and composition: background (BG), anthropogenic (ANT), and specific events (EV) that include advection of Saharan dust and upward transport from the polluted boundary layer to the site. On the basis of the presence or absence of coarse sea-salt particles, a further classification permits us to distinguish air masses that have or have not been exposed to the ocean. A closed mass balance is achieved on submicron ranges (mean departure of 18.5%) for the three main air mass categories, providing a reliable description of main aerosol types in the west European free troposphere. The total aerosol mass at 50% relative humidity is close to 2.7 ± 0.6 μg m^{-3} in BG, 5.3 ± 1.0 μg m^{-3} in ANT, and 15 to 22 μg m^{-3} in EV air masses. The aerosol mass distribution generally exhibits two submicron modes (Acc1 at 0.2 ± 0.1 μm and Acc2 at 0.5 ± 0.2 μm geometric mean diameter (calculated for every impactor stage) and a supermicron mode (2 ± 1 μm). Aerosols exhibit a high degree of external mixing with carbonaceous (EC and OC) and ionic species associated with Acc1 and Acc2. Concentrations of light carboxylates and mineral dust never exceed 4% of the total content of analyzed compounds, except for a Saharan dust event during which the contribution of insoluble dust reaches 26% of the total aerosol mass. Depending on the sampled air mass, bulk water-soluble inorganic species and carbonaceous material account for 25–70% and 15–60% of the total mass, respectively. The OC fraction is higher in air masses with low aerosol load (53%, 32%, and 22% for BG, ANT, and EV, respectively). Conversely, the EC fraction is enhanced from 4% in BG to 10% in ANT and 14% in EV. The inorganic fraction is more abundant in EV (55%) and ANT (60%) than in BG (40%) air masses as a result of enhanced nitrate and, to a lesser extent, sulfate and ammonium levels. *INDEX TERMS:* 0305 Atmospheric Composition and Structure: Aerosols and particles (0345, 4801); 0345 Atmospheric Composition and Structure: Pollution—urban and regional (0305); 0365 Atmospheric Composition and Structure: Troposphere—composition and chemistry; *KEYWORDS:* size segregation, aerosol, mass balance, organic carbon, free troposphere

Citation: Sellegri, K., P. Laj, F. Peron, R. Dupuy, M. Legrand, S. Preunkert, J.-P. Putaud, H. Cachier, and G. Ghermandi, Mass balance of free tropospheric aerosol at the Puy de Dôme (France) in winter, *J. Geophys. Res.*, *108*(D11), 4333, doi:10.1029/2002JD002747, 2003.

[1]Laboratoire de Météorologie Physique, CNRS, Université Blaise Pascal, Aubière, France.
[2]Laboratoire de Glaciologie et Géophysique de l'Environnement, St. Martin d'Hères, France.
[3]Joint Research Center, Ispra, Italy.
[4]Laboratoire des Sciences du Climat et de l'Environnement, CNRS, Gif sur Yvette, France.
[5]Dipartimento di Ingegneria Meccanica e Civile, Università di Modena e Reggio Emilia, Modena, Italy.

0148-0227/03/2002JD002747

1. Introduction

[2] Aerosol particles have both a direct effect on climate by reflecting and absorbing short-wave solar radiation and an indirect effect by influencing the optical properties and the lifetime of clouds. The uncertainty in quantifying both indirect and direct aerosol radiative forcing limits our ability to predict future surface temperature changes and to unambiguously detect a greenhouse-warming signal. At present, the global mean radiative forcing due to anthropogenic aerosol particles (direct and indirect effects) is estimated between -0.3 and -3.5 Wm^{-2}, which must be compared with the present-day forcing by greenhouse gases of +2.0 to +2.8 Wm^{-2} [*Intergovernmental Panel on Climate Change* (*IPCC*), 2001]. The aerosol (direct + indirect) forcing is therefore similar, but of opposite sign, to that due to greenhouse gases. However, because this forcing is spatially and temporally heterogeneous, it is a very complex scientific issue to quantify its effects at the global and local scales. A good knowledge of the aerosol properties from different areas of the world would clearly help regarding this issue.

[3] Regions under the influence of several aerosol sources are of great interest because very few information exist to characterize and unambiguously predict the degree of mixing of an aerosol population. The way different aerosol species are mixed in individual particles can, in fact, affect their optical and hygroscopic properties [*Heintzenberg and Covert*, 1990; *Jacobson et al.*, 2000]. To date, estimates of aerosol radiative forcing derive from atmospheric radiation models that assume externally mixed aerosols and that are sometimes based only on a simplified sulfate aerosol. This assumption has significant impacts on the calculated radiative properties by changing the single-scattering albedo that is generally different for internal mixtures of aerosols as respect to external mixtures [*Lesins et al.*, 2002]. This assumption is, however, only valid for very specific areas and often not adequate in places influenced by several aerosol sources where nonsulfate aerosol components account for a large fraction of the mass and have very different optical properties. In fact, direct and indirect evidences of internal mixtures between soot and sulfate have been published for different areas of the world [*Clarke et al.*, 1996; *Posfai et al.*, 1998; *Buseck and Posfai*, 1999].

[4] Not only does the state of mixing affect optical properties, but it also affects the particle phase and shape, since many thermodynamic factors, and in particular the deliquescent relative humidity, are largely dependent upon its chemical composition. Therefore the determination of aerosol chemical and physical properties in frontier regions is of great importance in understanding the effect of atmospheric particles in climate. Recent modeling includes now a more accurate description of the aerosol properties, but additional measurements of aerosol components are needed to validate the use of different aerosol categories in different areas.

[5] The evolution of polluted air masses advected into the marine atmosphere has been investigated during several field campaigns such as FETCH in Mediterranen Sea [*Sellegri et al.*, 2001], ACE-2 and ASTEX/MAGE in Atlantic Ocean [*Putaud et al.*, 2000; *Novakov et al.*, 2000; *Huebert et al.*, 1996] or INDOEX in the Indian Ocean [*Reiner et al.*, 2001]. Fewer data, however, are available on evolution of marine air masses transported inland and their interaction with primary and secondary anthropogenic and biogenic species. In Europe, background aerosol properties start to be documented for extended periods at several sites representative of marine, free tropospheric, rural and urban conditions. Long-term series are available at Mace Head representative for marine aerosol [*Jennings et al.*, 1997], Jungfraujoch [*Lavanchy et al.*, 1999] and Sonnblick [*Hitzenberger et al.*, 2000] for free troposphere, and rural sites in Finland [*Ricard et al.*, 2002], but less information from remote regions of western Europe is available.

[6] The free troposphere over western Europe is of interest as it can be considered as a zone where efficient long range transport takes place, as well as a mixing zone between marine air masses entering the European continent and air masses of continental origin, influenced or not by anthropogenic activities. The goal of this paper is therefore to provide information on the chemical and physical properties of aerosols in this area. Such a characterization will require, among others, an accurate determination of the chemical nature of particles including a size-dependent mass concentration of aerosol single components. We here present aerosol data gained at the Puy de Dôme station, located center of France at 400 km from the ocean and exposed to polluted air masses from northern Europe. Because clouds are often present at the site, these measurements are part of a more integrated approach to characterize the nucleating properties of the different aerosol types [*Sellegri et al.*, 2003]. The objective of the present study is to determine the physical and chemical properties of the major aerosol types in the free troposphere of western Europe in winter–spring. This was done in winters 2000 and 2001 by investigating mass closure and inorganic/organic partitioning in different aerosol types.

2. Site and Sampling Characteristics

2.1. Site Characteristics

[7] The experimental station is located at the summit of Puy de Dôme (48°N, 2°E, 1465 m above sea level). Meteorological parameters including wind speed and direction, temperature, pressure, relative humidity, and radiation (global, UV, and diffuse), gases (O_3, NO_x, SO_2, CO_2) and black carbon (BC) are monitored throughout the year. From October to April, access to the site is restricted to authorized persons, cars being stopped 5 km before the summit at 850 m (asl) elevation. A small military base is located north of the station, but fuel combustibles are exclusively used during storm winter events. Winter temperatures typically vary from -10 to $+10$°C and westerly and northerly winds are frequent although periods of southern winds can occasionally take place. Despite its relatively low-elevation, long-term records of gases and meteorological parameters indicate that in winter the site is mainly located in the free troposphere. That will be confirmed by the comparison of aerosol load and composition we made with other sites located at higher elevation in the Alps (Jungfraujoch, Sonnblick, Zugspitze) in sections 4 and 6.

[8] Data discussed in this paper are based on samplings achieved during two winter campaigns: from January to March 2000 and from February to March 2001. During the

Table 1. Experimental Conditions of Sampling During Field Campaigns PDD2000 and PDD2001[a]

Sample	Date	Cloudiness on Site, %	Duration	Impactor Type	Analyses Performed	Air Mass Origin (Time on Land)
1		85	67h30	ELPI10 ELPI20	IC $ECOC_{(a)}$	
2	15–18/02/00	100	65h40	ELPI10 ELPI20	IC $ECOC_{(a)}$	W (oceanic) (10)
3	18–21/02/00	65	67h30	ELPI10 ELPI20	IC $ECOC_{(a)}$	Mixed N/W (12)
4	21–22/02/00	0	26h	ELPI10 ELPI20	IC $ECOC_{(a)}$	N (Polar) (24)
5	22–24/02/00	40	40h	ELPI10 SDI ELPI20	IC PIXE $ECOC_{(a)}$	W/N (36)
7	25–28/02/00	20	65h	ELPI10 SDI ELPI20	IC PIXE $ECOC_{(a)}$	W–SW (20)
8	28/02–01/03	90	50h	ELPI10 SDI ELPI20	IC PIXE $ECOC_{(a)}$	S/W (60/6)
9	01–03/03/00	100	41h30	ELPI10 ELPI20	IC $ECOC_{(a)}$	NW/W (10)
10	04–06/03/00	50	43h10	ELPI10 ELPI20	IC $ECOC_{(a)}$	N (England) (32)
11	13–15/03/00	25	43h	ELPI10 SDI ELPI20	IC PIXE $ECOC_{(a)}$	N (Europe)/W (24)
12	08–09/02/01	100	18h45	ELPI20	IC	N (Europe)/W (24)
13	12–14/02/01	100	29h15	ELPI30 ELPI20	Mass/$OCEC_b$ IC	Variable (40)
14	15–16/02/01	0	20h	ELPI30 ELPI20	Mass/$OCEC_b$ IC	E (continent) (72)
15	16–17/02/01	90	20h	ELPI30 ELPI20	Mass/$OCEC_b$ IC	N/E (continent) (72)
16	17–18/02/01	100	21h20	ELPI30 ELPI20	Mass IC	NE (continent) (56)
17	19–20/02/01	20	20h50	ELPI30 ELPI20	Mass/$OCEC_b$ IC	N (Europe) (45)
18	22–23/02/01	100	21h10	ELPI30 ELPI20	Mass IC	NW (30)
19	23–24/02/01	100	9h05	ELPI30 ELPI20	Mass/$OCEC_b$ IC	NW (36)
20	28/02–01/03	100	25h50	ELPI10 ELPI30	Mass/$OCEC_b$ IC	W/N (12)

[a]Order in the impactor type is corresponding to order in the analysis performed on the corresponding impactor.

two campaigns, a complete set of aerosol (condensation nuclei counters, cloud condensation nuclei counters, filters, low-pressure impactors), cloud (size distribution, liquid water content), and gases (mist chambers) instrumentation was deployed at the site. Here, we will restrict our discussion to measurements related to the size-segregated aerosol composition. Table 1 summarizes achieved analyses and weather conditions (per cent of cloudiness and meteorological regime) encountered during sampling.

2.2. Particle Samplings

[9] Since clouds very often envelop the site, the aerosol sampling use a whole air inlet (WAI) which ensures efficient sampling of both cloud droplets and interstitial aerosols. WAI samples air at 12 m above the ground through a heated inlet that avoids ice formation. Air is sucked into a 12 cm-diameter PVC tube at a flow rate 30 $m^3\ h^{-1}$, subsequently subsampled inside the PVC tube with a 5 cm-diameter stainless steel tube (flow rate of 3 $m^3\ h^{-1}$) ensuring isokinetic subsampling. The stainless-steel section of the inlet is equipped with a heated section to evaporate cloud droplets and maintain relative humidity of sampled air at ~50% RH. Interstitial aerosols and evaporated cloud residues are sampled simultaneously at constant RH and can be compared in size regardless of the environmental conditions. Temperature never exceeded 25°C to limit aerosol volatilization. Wind velocity around the inlet head is lowered by a wind-shield. The sampled air is then isokinetically divided into 6 sampling lines for BC (aethalometer), cascade impactors, bulk filters (two lines), CCN chamber, CN counter and mist chambers (two lines).

[10] The WAI has been calibrated under clear sky conditions by running two particle counters inside and outside the inlet. Departures on the particle number concentrations were less than a few percents even when strong wind speeds (>15 m s^{-1}) took place. Under cloudy conditions, the calibration is performed by comparing the cloud liquid water content measured by a Particle Volume Monitor (PVM-100 Gerber) and the LWC calculated from relative humidity in the inlet and outside temperatures. Both data set show a good agreement except under high wind speeds (>15 m s^{-1}) and severe cloudy freezing conditions (temperature <−6°C). The overall sampling efficiency varies from 50 to 90%; losses are probably mostly due to inadequate sampling of large cloud droplets, which contain most of the water mass. Since cloud formation occurs frequently during winter–spring, care will be taken interpreting data on particles larger than a few microns.

[11] Particles are sampled using low-pressure cascade impactors. Three 13-stage ELPI impactors (commercialized by DEKATI Inc.) were run at 10 L min^{-1}, 20 L min^{-1} and 30 L min^{-1}, respectively, and a 12-stage SDI (Small Deposition Impactor [*Maenhaut et al.*, 1996]) impactor at 11 L min^{-1}. 50% cut-off diameters are 0.03, 0.06, 0.11, 0.17, 0.26, 0.41, 0.65, 1, 1.67, 2.5, 4.1, 6.9 and 10 to 10.6 μm for the ELPI impactors, and 0.045, 0.086, 0.153, 0.231, 0.343, 0.591, 0.796, 1.060, 1.660, 2.68, 4.08, and 8.39 μm for the SDI impactor. Cut-off diameters of the different impactors being not identical, comparison was done by running them with either identical or different substrates (see below). With respect to analytical uncertainties of chemical determinations the comparison between the two impactors indicates little differences between concentrations observed on the same size range, the disagreement being maximum for species like formate, acetate and potassium which are present at low levels on first and last impactor stages. Stage to stage correlation between total inorganic concentrations measured with both impactor types give the relation ELPI = 1.28 * SDI − 6.6 (ng m^{-3}) with a R^2 = 0.87, and the disagreement is less than 15% on the bulk (all stages) concentration.

[12] Employed impaction substrates were different depending on investigated chemical species. In order to minimize blank values in particular for organic matter, none of these substrates was coated with grease as commonly used to prevent from bouncing of particles. Bouncing is maximum for large and dry particles [*Hinds*, 1998], thus as sampling is performed at relatively high RH imposed in the WAI (typically 50%), it should remain limited in the

Table 2. Detection Limits of the Analyzed Species Calculated for a Typical 20 h/26 m^3 Sample, per Impactor Stage, as Blank Concentrations Plus Standard Deviation

	Detection Limit, ng m^{-3}/stage																
	Ace	For	Cl^-	NO_3^-	SO_4^{2-}	Ox	Na^+	NH_4^+	K^+	Mg^{2+}	Ca^{2+}	OCEC	EC	Al	Si	S	Fe
Polycarb.	1.7	0.8	3.7	1.7	2.63	0.23	2.2	0.87	0.63	1.42	5.35						
Teflon	1.78	0.17	0.45	2.91	0.27	0.08	0.36	0.04	0.35	0.02	0.24						
Aluminum (ECOC)/Polycarbonale (PIXE)												67	5.9	9.3	0.6	1.1	0.1

submicron ranges. Note that the use of uncoated impaction substrates would limit gas absorption.

[13] Teflon filters (Nuclepore, 0.2 μm pore size) were used for ion chromatographic analysis in 2000, polycarbonate filters (Nuclepore) for PIXE and ion chromatography in 2001. Aluminium foils used for OC, EC and gravimetric measurements were washed with ultrapure water and methanol and then dried under a class 100 laminar flow bench.

[14] Impactor substrates were loaded and unloaded in the field under a clean air bench equipped with an active charcoal filter to limit contamination by HNO_3 or NH_3 vapors. Samples are stored in individual airtight petri dishes (Analyslides®) and kept frozen until analyses. Blanks are performed on a regular basis throughout the campaign (typically 1 blank for each impactor sample) by loading and unloading a substrate using the same procedure as for real samples. All concentrations given in this paper have been corrected for blank levels.

3. Analyses

[15] With the aim to provide a comprehensive chemical study of the different aerosol population present at Puy de Dôme in winter analysis include total aerosol mass, ionic species, EC and OC, and elemental species.

3.1. Total Mass of Aerosol

[16] Gravimetric measurements are performed using a MSO1 Mettler microbalance placed in a class 10 000 clean room where constant relative humidity (50 ± 10%) and temperature (20°C) are maintained. The balance sensitivity is 0.1 μg and an accuracy of 0.4 μg is found by repeated weighting of the same filter. Aluminum foils were used for black and organic carbon analyses after gravimetric measurements. A mean blank value obtained by performing measurements of 10 aluminum foil blank is slightly negative (0.29 μg) possibly because of electrostatic effects and micro-loss of foil material during handling. From that we estimate a detection limit close to 0.4 μg leading to a mean uncertainty lower than 7% for particles between 0.14 to 0.8 μm diameter, 15% for particles smaller than 0.14 μm and 30% for particles larger than 0.8 μm (because they represent lass mass). An estimate of the influence of water present on filter was done by applying a typical growth factor of particles at 50% RH. Most of hygroscopic particles (sea salt) show growth factors slightly larger than 1 up to 70% RH and close to 1.5 with decreasing RH from wet state to 50% due to hysterisis [*Hansson et al.*, 1998]. At 50% RH, Ammonium sulfate particles have growth factors of 1 with increasing RH and 1.1–1.2 for decreasing RH [*Hämeri et al.*, 2000]. Because we do not know what growth factor is associated to carbonaceous material, and in order to avoid overestimating the amount of water associated with the particles, an intermediate growth factor (between increasing and decreasing RH) of 1.02 was chosen for submicron sizes. Since gravimetric determinations have been only performed in 2001 when supermicron particles were rarely detected, the expected larger artifact due to hygroscopic growth of coarse sea-salt particles will be limited. The water content associated with weighed particles could be higher thus limiting the amount of undetermined species in the mass balance.

3.2. Ion Chromatography

[17] Filter extraction and IC analyses are performed inside a clean room (class 10 000). Polycarbonate filters were extracted with ultrapure water and Teflon filters with a 10% mixture of methanol/Milli-Q water (18.2 μS). The extracted liquid is analyzed by ion chromatography using a DIONEX 100 chromatograph equipped with a CS12 column for cations, and a DIONEX 500 chromatograph with an AS11 column for anions. Analyzed species are CH_3COO^-, $HCOO^-$, Cl^-, NO_3^-, SO_4^{2-}, $C_2O_4^{2-}$ (oxalate here abbreviated Ox), Na^+, NH_4^+, K^+, Mg^{2+}, and Ca^{2+}, using working conditions detailed by *Ricard et al.* [2002]. Atmospheric detection limits taken as mean blank plus one standard deviation, calculated for an averaged air sampled volume of 25 m^3, are reported in Table 2. The accuracy of IC is typically 10% for samples 10 times the detection limit and ~50% for samples 2 times the detection limits.

3.3. Carbon Analysis

[18] Aluminum substrates were analyzed for carbon after gravimetric analyses (only done in 2001). In 2000, measurements were done using the analytical protocol described by *Cachier et al.* [1989]. After removal of carbonate, samples are left at 340°C during 2 hours under pure oxygen. EC and TC (Total Carbon, TC = OC + EC) are then determined on aliquots of the same substrate by coulometric titration using a Ströhlein Coulomat 702C analyzer, with a precision close to 10%. In this study, only TC has been determined.

[19] Using the protocol described by *Putaud et al.* [2000], EC and OC were determined on 2001 samples by using a thermal method where samples are exposed to increasing temperature in an O_2 content controlled carrier gas. Carbon matter is volatilized and decomposed into a carbon-containing gas, further converted into CO_2 over a CeO_2/CuO catalyst maintained at 900°C. CO_2 is detected by a non-dispersive infrared analyzer. The analytical method applied to 2001 samples slightly differs from the method used by *Putaud et al.* [2000] during ACE-2 in the following steps: samples are heated at a rate of 600°C per minute from 80 to 100, 110 to 220, 220 to 330°C in a He-O_2 80:20 mixture leading to three separate peaks labeled OC1.1, OC1.2 and OC1.3 (Organic Carbon). Then it is heated with the same gradient from 330 to 440, and from 440 to 650°C in pure He

(to limit charring) leading to two separate peaks labeled OC2.1 and OC2.2. Finally, oxygen is mixed to helium again with a mixing ratio of 10% at 650°C then the temperature is raised to 750°C. The two peaks observed during this step are defined as EC1 and EC2 (Black Carbon). One source of error in carbon analysis is charring of OC into EC as reported by *Chow et al.* [1993]. Organic carbon charring has been evaluated on two samples (samples 14 and 15) by analyzing one half of each impactor stage after exposure to an oxidized atmosphere at 340°C. The difference between the routine analysis and the 340°C analysis represents the amount of charred OC and is dependent on particle size. We found that charred OC is well correlated to EC level (R^2 is 0.94 for 26 points, and $OC_{charred} = 0.282*EC$). On this basis, $OC_{charred}$ is calculated from EC concentrations using the following correction:

$$OC = OC_{measured} + OC_{charred,\ calculated}$$
$$EC = EC_{measured} - OC_{charred,\ calculated}$$

[20] The measured relationships between $OC_{charred}$ and EC show 15% variability between the different samples. Thus, using correction factors to samples for which charring is not directly evaluated leads to an additional 4% uncertainty on the EC concentrations. The additional uncertainty on the OC concentrations is negligible. Blank levels per impaction substrate are 1.57 ± 0.17 and 1.62 ± 0.36 μg C in 2000 and 2001 samples, respectively. The precision given by *Putaud et al.* [2000] is better than ±8% for TC and the accuracy derived from intercalibration is ~20% for TC and 60% for BC. For the purpose of this paper, only EC and OC level will be discussed, speciation of OC into different volatility classes being discussed elsewhere [*Sellegri et al.*, 2003].

[21] Several previous studies have pointed out a possible artefact due to sticking of organic vapors onto filters during sampling [*McDow and Hnutzicker*, 1990; *Turpin et al.*, 1994]. The use of an impactor would minimize such a sampling artifact [*Turpin et al.*, 1997; *Saxena and Hildemann*, 1996] since organic vapors condense less easily on impactor substrates than on filters, even though significant positive artifacts have been found on SDI cascade impactors in the urban atmosphere [*Viidanoja et al.*, 2002]. Conversely, examination of the size-segregated aerosol composition may help to identify the occurrence of such a phenomenon since for a purely aerosol derived species we can expect a distinct mass distribution with size. Among all investigated chemical species, only some carboxylates (formate and acetate in contrast to oxalate) and the most volatile fraction of OC (OC1.1) exhibit no variation of concentrations with size. Their concentrations being close to detection limits, we cannot conclude that there is an artifact resulting from sticking of these organic gases onto impactor stages. However, if OC1.1 represents the amount of organic gases absorbed onto the impaction substrates, it accounts for less than 1% of total OC.

3.4. Particle Induced X-Ray Emissions (PIXE)

[22] Elemental species have been measured by PIXE analysis following analytical procedures developed at the University of Modena. The incident particles are protons accelerated to 1.8 MeV by a Van de Graaf accelerator at the National Laboratory at Legnaro (Padova, Italy). To obtain an homogeneous circular beam spot at the target, the beam is diffused through a Ni foil (450 μm cm^{-2}) then carbon collimators pick off the central part of the beam (~1.5 cm diameter). The Si (Li) detector (the same type used in the microPIXE set up) is placed at 135° from the beam in front the target. Under these conditions the X-ray attenuation in the target is also limited. A 50 μm mylar absorbers with a central hole (equivalent to 7.5% of the total area) was placed in front of the detector during aerosol analysis to partly attenuate the low-energy X-ray intense emissions. The PIXE measurement of sample was performed with a diffused beam, collimated to produce a 1,77 cm^2 spot (i.e., irradiated sample area) on the target. Each sample stopped after collection of 16 μC of charge on the target during exposition to the proton beam, with current of about 12 nA. Blank targets (Nuclepore membrane) were measured under the same conditions. The software used for PIXE spectra analysis and element concentration evaluation is GUPIX 4, which also estimates errors (typically <15%) and detection limits tens to 0.1 ng m^{-3} (Table 2).

[23] Analyzed species are Na, Mg, Al, Si, P, S, Cl, K, Ca, V, Ti, Fe, V, and Mn. For the purpose of this study, we focus on aluminum, iron, and silicon, which dominate the analyzed mass with this method, and S, which can be compared to sulfate ion chromatograph data. The insoluble crustal contribution is defined as the sum of Al_2O_3, FeO, SiO_2, as they are the most significant oxides found in the continental crust [*Weast*, 1984]; in the following, "dust" will refer to the sum of Al_2O_3, FeO and SiO_2, calculated from the measured Al, Fe and Si PIXE concentrations. Detection limits per impactor stage calculated as the mean detection limit for all analyzed samples and a mean sampled air volume of 25 m^3 are reported in Table 2.

[24] Comparison between IC and PIXE measurements has been performed for Sulfur. On average we find a reasonably good agreement between elemental sulfur and sulfur derived from sulfate IC measurements (mean 15%). For calcium, which is very likely present in a soluble form (gypsum and $CaCO_3$), PIXE data are, again, 15% lower than ion chromatography data. That remains, however, consistent given the uncertainties of the 2 methods for low calcium levels encountered at this site.

4. Aerosol Types at Puy De Dôme

[25] Chemical analyses and gravimetric data are reported in Table 3. In order to identify the different aerosol types that reached the Puy de Dôme station (PDD) during the two winter seasons, we first examine the sum of inorganic ions, which have been investigated in all samples (Table 3). The median value of the sum of ions is close to 1530 ng m^{-3} (with 730 and 1950 ng m^{-3} for 25th and 75th percentiles, respectively). Sulfate, nitrate and ammonium represent together 80% of the sum of ionic species. Based on that, we performed a first clustering of samples into two different classes, "background free tropospheric aerosols" (denoted BG) characterized by ionic content lower than 1 μg m^{-3} (samples 1, 2, 3, 13, 18, and 20, see Table 3) and "anthropogenic influenced free tropospheric aerosols" (denoted ANT) whose the ionic content ranges between 1 and 2.2 μg m^{-3} (samples 4, 5, 7, 8, 9, 10, 14, 16, 17 and 19,

Table 3. Bulk Concentrations of Analyzed Species[a]

Sample	Sample 1	2	3	4	5	7	8	9	10	11	13	14	15	16	17	18	19	20	Mean	Std. Dev.	Median	25th Percentile	75th Percentile
Air mass type	BGM	BGM	BGC	ANTC	ANTC	ANTC	ANTM	ANTM	ANTM	EVM	BGC	ANTC	EVC	ANTC	ANTC	BGC	ANTC	BGC					
$HCOO^-$	8	0	3	0	24	0	23	18	8	42	8	29	35	16	15	17	7	19	14	12	15	6	20
Cl^-	399	131	49	0	0	0	40	192	81	45	16	15	0	12,1	39	0	75	0	56	92	18	0	56
NO_3^-	88	195	92	419	734	623	421	506	909	4413	191	579	4757	519	397	198	800	207	821	1278	420	197	651
SO_4^{2-}	161	134	399	446	601	742	736	796	563	1789	292	975	4066	728	1089	156	722	323	765	850	582	315	756
Ox	0	5	9	10	48	175	34	105	23	70	14	40	144	19	8	16	26	16	39	47	18	12	42
Na^+	268	108	51	51		30	105	194	229	186	20	24	149	33	88	3,6	117	23	90	78	51	24	133
NH_4^+	38	42	142	247	72	215	422	148	297	712	120	253	1535	292	513	106	329	131	293	330	209	117	305
K^+	9	4	5	13	16	29	26	26	18	104	4	22	95	10	23	4	10	2	21	27	12	5	24
Mg^{2+}	65	25	9	7	2	3	10	14	56	37	2	117	118	9,1	0	19	0	0	25	36	9	2	28
Ca^{2+}	13	6	0	5	15	16	27	19	30	325	2	47	230	15	23	32	0	0	40	81	15	4	28
sum inorg	976	477	739	1182	1443	1658	1777	1893	2129	7577	645	1919	10846	1612	2201	500	2056	688	2080	2502	1527	726	1953
OA. Ceq	10	5	5	3	23	48	20	56	8	65	7	26	138	12	43	9	12	12	26	31	12	8	30
Al_2O_3					78	45	88	63		1515									358	579	78	63	88
SiO_2					67	78	51	11		2977									637	1170	67	51	78
FeO					49	23	6	1		401									96	153	23	6	49
ECOC	1110	1520	870	1820	1300	1220	1100	650	236	1800	2030	2900	8060		2140		1720	1565	1878	1710	1543	1108	1873
EC											110	722	2900		725		275	125	810	969	499	163	724
OC											1930	2176	5160		1410		1445	1445	2261	1328	1688	1445	2115
sum.,[b] $\mu g\ m^{-3}$				3.0	2.95	3.04	3.04	2.66		14.3	2.67	4.82	18.9	1.61	4.34	0.50	3.78	2.25	4.85	4.98	3.02	2.67	4.2
Gravim., $\mu g\ m^{-3}$											3.39		22.0	3.9	6.10	1.94	5.89	2.75	6.56	6.46	3.86	3.07	6.0

[a]Bulk concentrations are given in ng m^{-3}. Note that while ECOC mean concentration is calculated on all samples, EC/OC discrimination is only available PDD2001 samples.
[b]Polyinorganics + OCEC + dust.

see Table 3). Samples 11 and 15 (7.6 and 10.9 μg m^{-3}, respectively) clearly display from this classification and will be designed as "Event" (EV). On the basis of the ionic species load this classification is consistent with the total mass derived from gravimetric analyses for 2001, the total mass of aerosol ranging from 1.9 to 3.4 μg m^{-3} for BG, 3.9 to 6.1 μg m^{-3} for ANT and 22 μg.m^{-3} for EV.

[26] A further classification can be proposed from the examination of the aerosol mass size distribution of ionic species reported in Figure 1 for BG, ANT and the two EV samples. In each class of samples, some clearly exhibit a bimodal (submicron and supermicron) distribution and others a mono modal distribution dominated by the submicron mode. When present, the supermicron mode is mainly made of Na and Cl (see the case of samples 1 and 2 for BG and samples 9 and 10 for ANT reported in Figures 1a and 1b, respectively, and corresponding sodium level higher than 100 ng m^{-3} in Table 3) or nitrate (see sample 15 reported in Figure 1c for which the nitrate level is close to 5 μg m^{-3}, Table 3). That suggests the final classification into BG, ANT and EV with the presence (BGM, ANTM and EVM) or absence (BGC, ANTC and EVC) of marine input summarized in Figure 2.

[27] The sum of quantified (organic and inorganic) species concentrations or, when available, the total mass derived from gravimetric analysis indicates total aerosol mass in the range of 2 to 6 μg m^{-3} with exceptionally high values for sample 11 (14 μg m^{-3}) and sample 15 (close to 20 μg m^{-3}) (Table 3). Discarding the case of sample 11, which as discussed below can be attributed to a long-range transported Saharan dust input reaching the site, the total aerosol mass of sample 15 falls in the range of levels usually characterizing the boundary layer (from 8 to 37 μg m^{-3} for instance in Chicago [*Offenberg and Baker*, 2000], 20 μg m^{-3} in a rural Hungarian site [*Temesi et al.*, 2001]). The total aerosol mass of 2 to 6 μg m^{-3} seen for BG and ANT samples is consistent with typical remote levels reported by *Heintzenberg* [1989] (4.8 μg m^{-3}). More specifically, the total aerosol mass at PDD is comparable to total mass observed at higher-elevation sites located in the Alps (3.1 ± 1.7) at Jungfraujoch at 3250 asl in Switzerland [*Krivacsy et al.*, 2001].

5. Aerosol Mass Closure

[28] Analyses including gravimetric data, inorganic ions, EC, and BC are available for samples 13, 15, 17, 19 and 20 that correspond to BG (samples 13 and 20), ANT (samples 17 and 19) and EV (sample 15). For these samples, a mass closure can be examined by comparing gravimetric and chemical analyses (see Figure 3). That requires that we evaluate the amount of water present on filters, the amount of insoluble dust not investigated by ion chromatography, as well as the knowledge of the conversion factor between organic matter and organic carbon mass. Sampling has been performed at 50% RH, we have applied a growth factor of 1.02 (see section 3.1). That leads to a mass of H_2O that is approximately 3% of total mass. The dust contribution can be derived from PIXE data available on samples 5, 7, 8, 9, and 11. On the basis of Si, Al, and Fe levels we have calculated total mass of dust as the sum of Al_2O_3, SiO_2, and FeO (see section 3.4). The ratio between dust and total inorganic bulk concentrations is always lower than 6.5% except for sample 11 that clearly originates from the advection of Saharan air masses to Europe as suggested by the red-looking aspect of corresponding impaction substrates. On the basis of this value of 6.5% and using the total

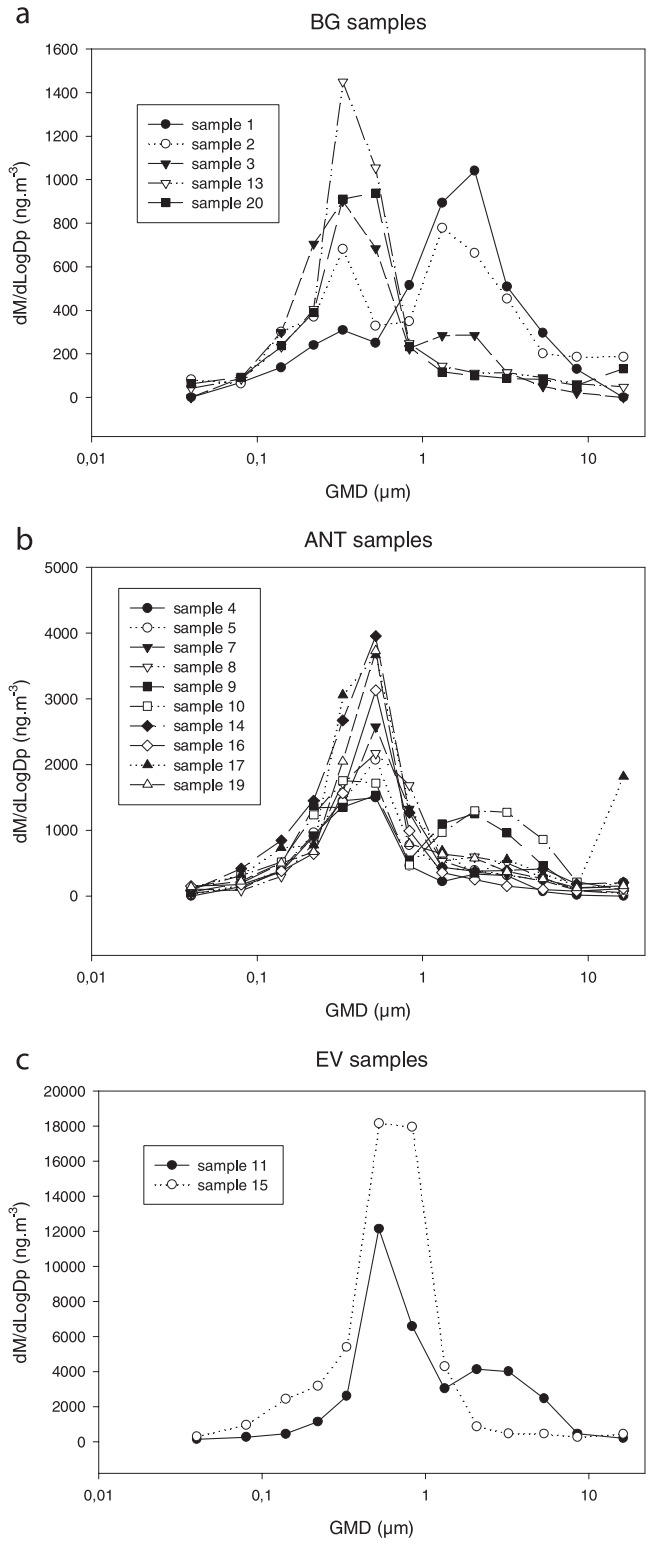

Figure 1. Mass size distributions of inorganic components for (a) BG, (b) ANT, and (c) EV samples.

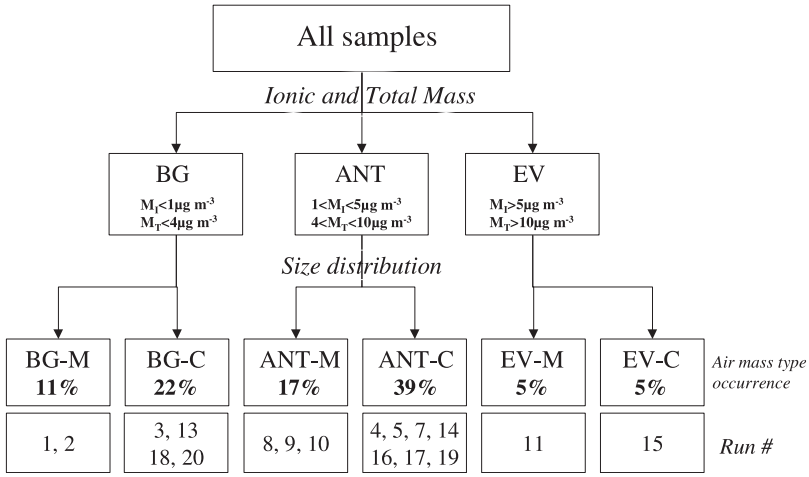

Figure 2. Winter type aerosol classification.

amount of inorganic species, we have estimated the dust contribution for samples 13, 17, 19, and 20 (obviously not originating from Saharan dust events from their nss-Ca content and mass size distribution).

[29] As seen in Figure 3, when a OM/OC conversion factor of 1 is assumed, the difference between calculated (ion + dust + EC + OC) and measured (gravimetry) total aerosol mass corrected from water total mass is of 21% for particles belonging to the first accumulation mode (GMD of 0.2 µm) and 19% for the second accumulation mode (GMD of 0.5 µm) (GMD is geometric mean diameter, calculated for each impactor stage (i) from the cut-off diameter Dp_i as GMD_i = square roots (Dp_i * Dp_i + 1) [*Hinds*, 1998]; note that the upper inlet cut-off diameter is arbitrary set to 25 µm). The OC/OM conversion factor required to close the mass balance varies from 1.2 at 0.30 µm GMD to 2.5 and 4 for particles of 0.08 µm GMD and 0.8 µm GMD, respectively. Conversion factors found in the literature are usually of 1.2 for water insoluble OC and 1.4 for water soluble OC [*Zappoli et al.*, 1999], although recent estimations suggest that values of 1.6 and 2.1 are more accurate [*Turpin and Lim*, 2001] for water insoluble OC and water soluble OC. Applying a value of 1.2 found on impactor stages containing a high carbonaceous aerosol load (~0.33 µm), we obtain a mass closure achieved within 18.5% of the total mass (6, 20, and 7.5% for BG, ANT and EV, respectively). The higher departures in ANT air masses would suggest the presence of a larger fraction of water soluble OC there. Inversely, if a OC-to-OM conversion factor is calculated from mass closure on the bulk concentrations, we find 1.2 for BG, 3.1 for ANT and 1.3 for EV samples, indicating a higher degree of oxidation of OC in ANT samples. From these calculations, our results would be closer to the findings of [*Turpin and Lim*, 2001] specifically for the ANT samples, although our method to come to these values is different from theirs. The disagreement between gravimetric and chemical determination masses is also higher for coarse particles suggesting a higher OM/OC ratio for these particles but the higher uncertainty on measurements prevents to conclude. Anyway, we can conclude that submicron particles in the free troposphere are well described by ion and carbonaceous analyses.

[30] Achieved size-segregated mass closure of aerosols present over continents is uncommon in literature. Achieving a mass closure on 4 size fractions during ACE-2 in Portugal reached 98% agreement between chemical and gravimetric mass for particles between 0.05 and 3.5 µm [*Neusüß et al.*, 2000]. Such a good agreement was due to a very low carbonaceous contribution (~6%) and consequently a small impact of the employed OC to OM conversion factor. *Putaud et al.* [2000] found agreement between mass concentration derived from chemical measurements and calculated from the number size distribution within 45% for the marine boundary layer and within 75% for the free troposphere. *Temesi et al.* [2001] recently achieved a size-segregated mass balance in rural atmosphere by measuring ion and total carbon concentrations along with total number concentrations. They found a significant portion of unaccounted mass (22%) after water content correction and applying an OM/OC conversion factor of 1.8. The discrepancy was at least partly attributed to assumptions made in calculating the mass concentration from number concentration according to which particles have unit density.

6. Chemical Signature of the Different Air Masses

[31] In this section we discuss main chemical characteristics of different aerosols encountered at PDD in winter. That will be done in the light of the respective contributions of EC, OC, ionic (inorganic and carboxylates) species, and mineral dust to the total aerosol mass reported in Figure 4. The contribution of each aerosol component is calculated as its ratio to the sum of inorganic, dust (when available) and carbonaceous contents. The nonidentified (nd) fraction is calculated from the weighted mass (corrected for H_2O contribution) when gravimetry data were available. We will also examine the size distribution of each aerosol components (inorganic, carboxylates, carbonaceous, and dust) as reported in Figures 5–8 (see also Table 4).

6.1. Inorganic Species

[32] As already mentioned in section 4, the sum of inorganic ions is dominated by ammonium, sulfate and

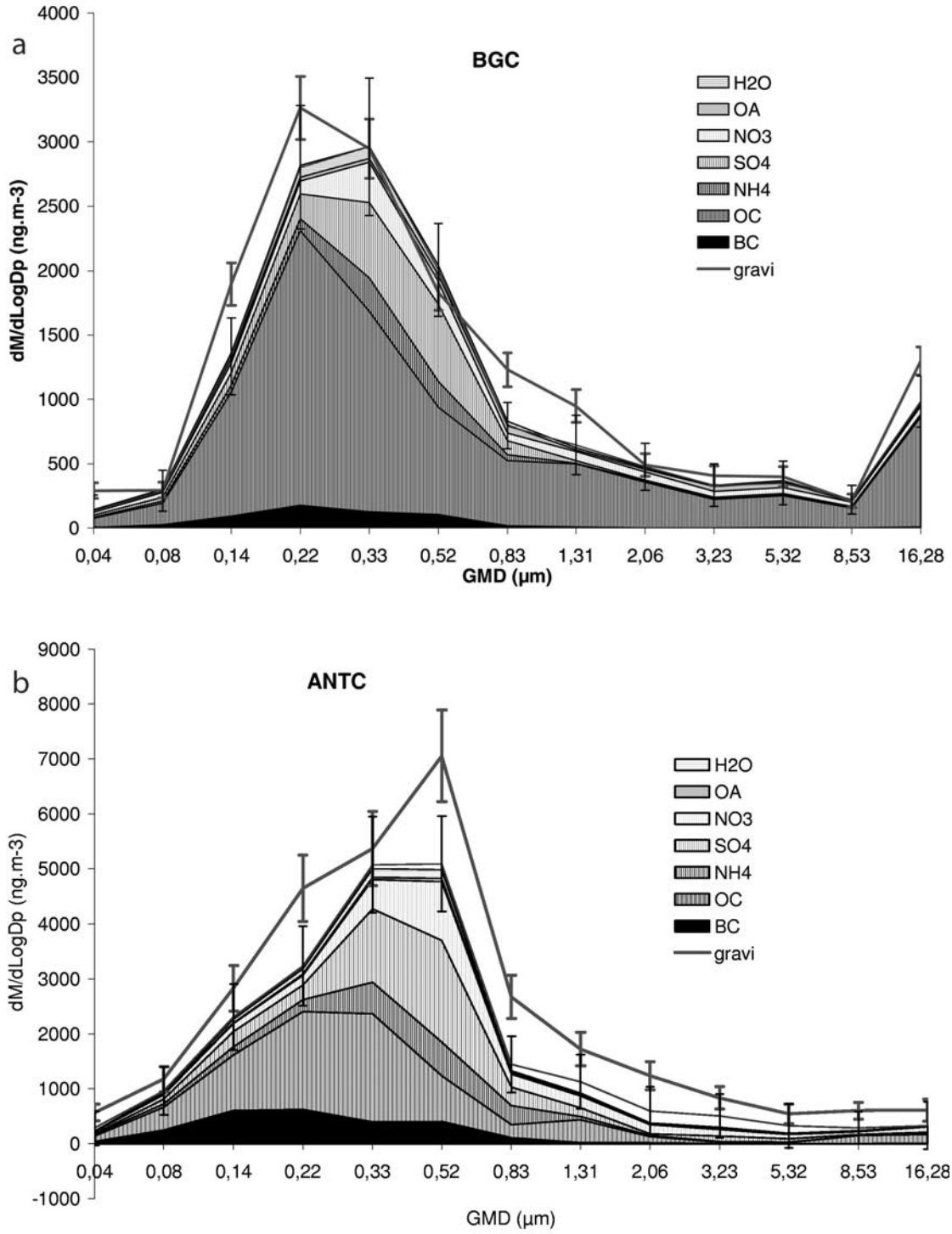

Figure 3. Mass closure of mass size distributions for (a) BG, (b) ANT, and (c) EV samples. Note that OC and BC are reported as ng m^{-3} of C.

nitrate with a mean concentration of $SO_4^{2-} + NO_3^- + NH_4^+$ ranging from 0.43 ± 0.09 μg m^{-3} for BGM, 0.64 ± 0.07 μg m^{-3} for BGC, 1.9 ± 0.3 μg m^{-3} and 2.0 ± 0.3 μg m^{-3} for ANTM and ANTC, reaching 13.6 μg m^{-3} for EVC. These BG and ANT values are in the range of those observed at the high alpine site of Sonnblick (Austria) where monthly averaged winter concentrations for the sum of sulfate, nitrate and ammonium vary from 0.5 to 3 μg m^{-3} from January to March 1992–1993 [*Kasper and Puxbaum*, 1998].

[33] Sulfate which represents 35 ± 7% of inorganic ion mass varies from 0.3 ± 0.1 μg m^{-3} in BG to 0.8 ± 0.15 μg m^{-3} in ANT, EVM and EVC samples exhibiting sulfate levels higher than 1.8 μg m^{-3}. Except for BGM samples

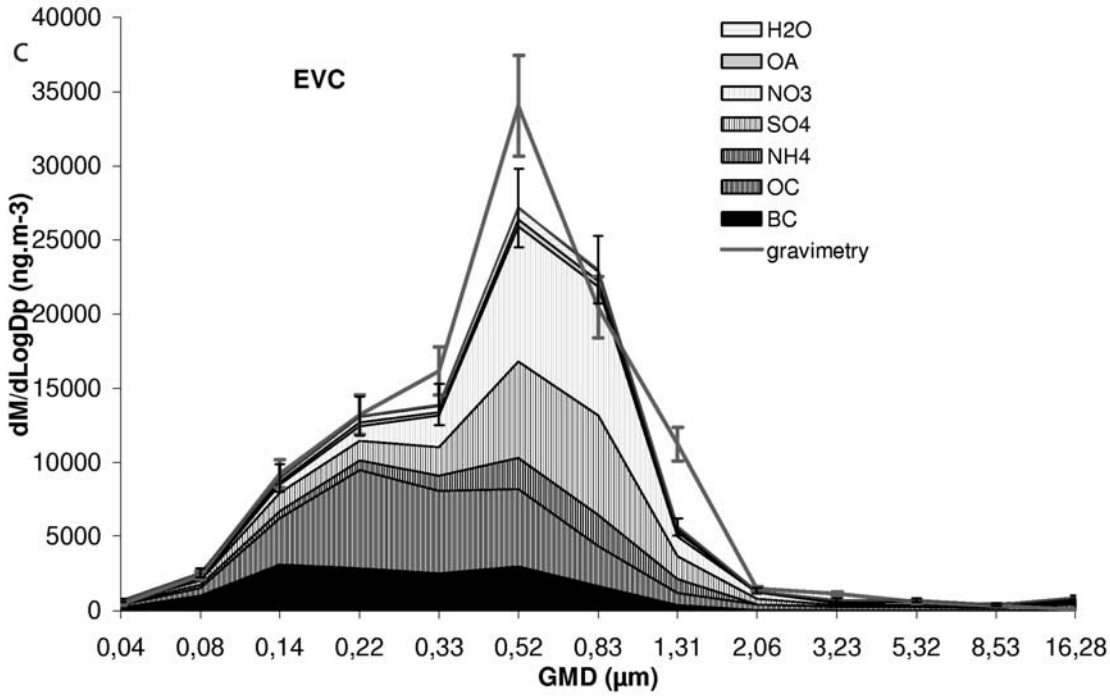

Figure 3. (continued)

characterized by relatively high sea-salt contents and for which sea-salt sulfate accounts for 20 to 40% of total sulfate, sulfate is mainly (>90%) present as non-sea-salt sulfate. In the EVM sample, which contains Saharan dust, a part of sulfate may be present as gypsum. A S/Ca mass ratio of 0.15 (i.e., a sulfate to calcium ratio of 0.44) is observed with PIXE analysis at 2 μm in EVM. Note that this value is consistent with the mean one proposed by *Wagenbach et al.* [1996] and *Preunkert et al.* [2001] for Saharan dust plumes reaching the Alps (0.59). Using the value of 0.15 and referring to the calcium content of EVC (325 ng m^{-3}, Table 3), we calculate that only 8% of sulfate would be related to the presence of gypsum there. BG and ANT air masses at PDD exhibit sulfate levels that are slightly lower than the monthly average sulfate levels at Sonnblick (0.75 to 1.9 μg m^{-3} in February and March 1992–1993; *Kasper and Puxbaum* [1998]) and at Schwainsland (1205 m asl, black forest in Germany) (2 μg m^{-3} in winter 1991–1993, see *Preunkert et al.* [2001]). A Part of this difference is likely due to the decrease of SO_2 emissions that have taken place from 1980 to present as a result of improvement in the quality of fuel and emissions abatements. Note also that as predicted by model simulations (see *Barth et al.* [2000], for instance) we can expect lower anthropogenic sulfate levels in the western flank of Europe than in more central site like Sonnblick.

[34] Nitrate concentrations vary from 0.16 ± 0.05 μg m^{-3} in BG to 0.61 ± 0.16 μg m^{-3} in ANT, EV samples exhibiting levels higher than 4 μg m^{-3}. On average, nitrate is the second major contributor to the ionic mass for BG and ANT (28 ± 8%) and the first one for EV (49 ± 9%). The mean nitrate level in BG and ANT at PDD is of the same order of magnitude than the mean particulate nitrate level observed at Sonnblick (0.07 and 0.5 μg m^{-3} for February and March 1992–1993; *Kasper and Puxbaum* [1998]) (note that in contrast to sulfate no major change of nitrate is expected between 1992–1993 and present-day because of an absence of reduction in NOx emissions). With 4.4 μg m^{-3} nitrate levels in EVC are similar to the EVM one. Such a high level of nitrate in EVC suggests a strong neutralization of calcite present in the Saharan material during its transport to the site as already noticed by *Maupetit and Delmas* [1994].

[35] Finally, with levels ranging from 0.10 ± 0.04 μg m^{-3} in BG to 0.28 ± 0.13 μg m^{-3} in ANT, ammonium at PDD is comparable to the situation at Sonnblick with concentrations of 0.2 and 0.6 μg m^{-3} in February and March 1992–1993 [*Kasper and Puxbaum*, 1998]. Its contribution to the ionic mass remains close to 15 ± 5%.

[36] As shown in Figure 5, sulfate and ammonium are present in the submicron mode located on particles ranging from 0.3 to 0.8 μm GMD (Acc2 mode). The GMD of Acc2 varies from 0.3 μm to 0.83 μm depending on event. This difference cannot be caused by changing RH in the inlet since RH is controlled around 50% and aerosol growth does not take place in the low-pressure impactor [*Howell et al.*, 1999]. In the literature, the accumulation mode has sometime been split into condensation mode (0.25–0.35 μm) resulting from growth by condensation and droplet mode (0.5–0.8 μm) resulting from aqueous growth of the condensation mode [*Kerminen and Wexler*, 1995; *Meng and Seinfeld*, 1994]. However, from sample 3 to 8, the total particle mass increases without significant changes in the chemical composition of Acc2, except an increasing proportion of nitrate. We therefore propose that air masses are getting more processed from sample 3 to 8 with gaseous species, dominated by HNO_3, condensable onto the particles.

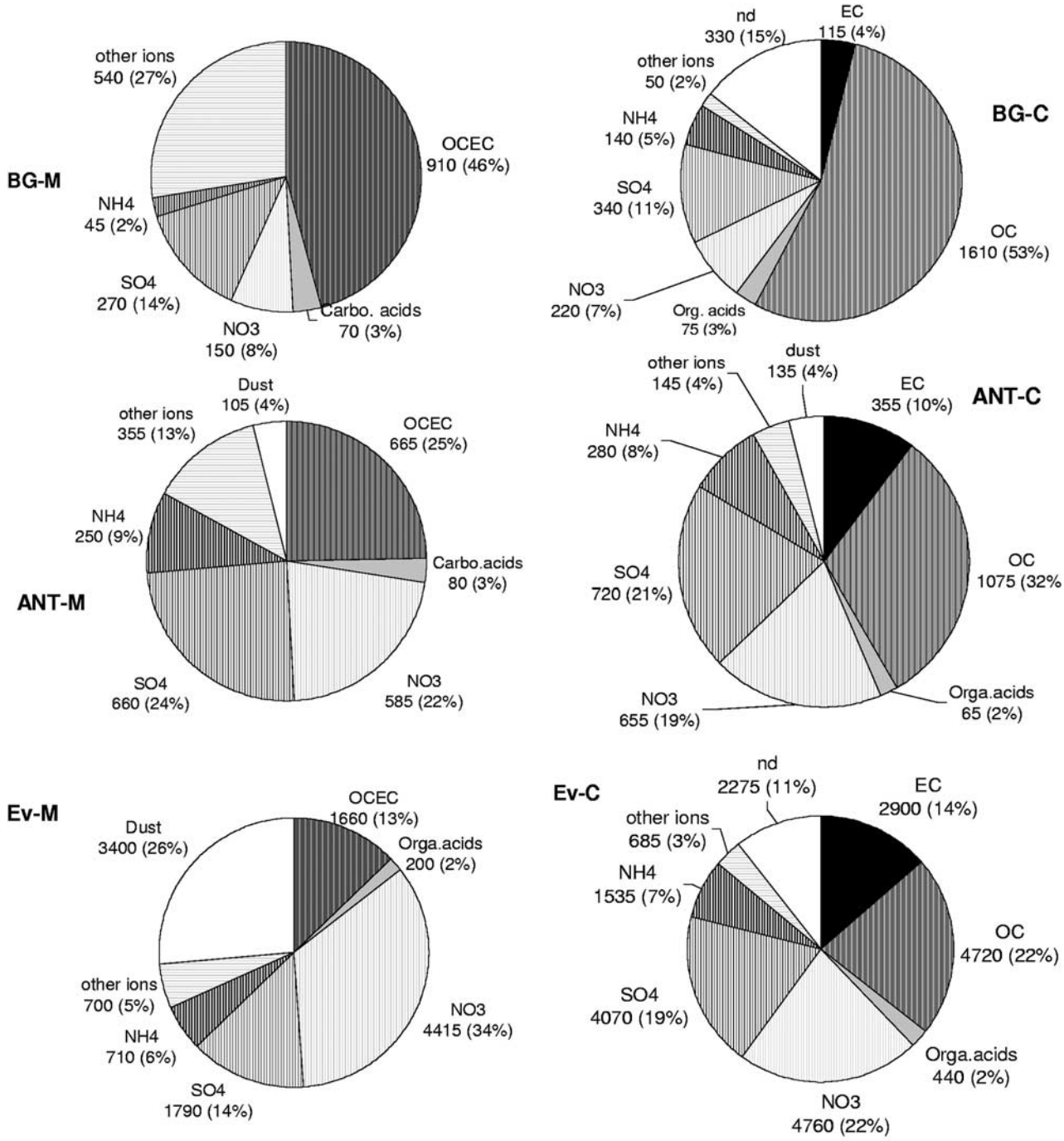

Figure 4. Bulk aerosol composition (in ng m^{-3}) for the six different types of aerosols (see text). Numbers under parenthesis correspond to percentages of total mass.

[37] In contrast to sulfate and ammonium, nitrate is present both in the accumulation and the coarse particle modes. Some samples are bimodal while others only show either an accumulation or a coarse mode. For winter 2000 characterized most of time by marine influence we observe that nitrate is bimodal in 80% of samples. On the contrary, the bimodality of nitrate has not been observed in 2001 predominantly influenced by continental air masses. The apportionment of nitrate between submicron and supermicron modes is variable (subratio to total ratio ranging from 63 to 96%) with a higher proportion of submicron nitrate for continental samples (ANTC and EVC).

[38] Stage to stage correlation on submicron stages of impactor is better between nss-SO_4^{2-} and NH_4^+ ($R^2 = 0.9$) than between NO_3^- and NH_4^+, suggesting a favored formation of ammonium sulfate (or bisulfate) over ammonium nitrate. BG samples generally show an ammonium to sulfate slope lower than unit whereas for ANT samples a slope closer to unit or more is observed (mean NH_4^+/nss-SO_4^{2-} 0.8 for BG samples, and 1.15 for ANT samples). For the samples

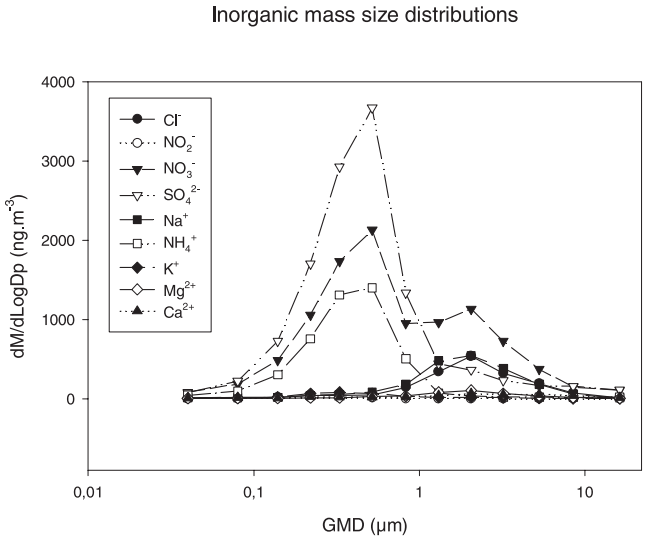

Figure 5. Mass distribution for inorganic ions for all analyzed samples.

containing a high amount of ammonium, we found a correlation coefficient R^2 of 0.65 between the excess of ammonium ($NH_4^+ - NH_{4\,\text{associated with SO4}}^+$) and submicron nitrate. That suggests the occurrence of either reaction between HNO_3 and NH_3 or reaction of HO_2 on NO_2 producing gaseous HNO_4, which is rather highly soluble in water [*Warneck*, 2000].

[39] The concentration of other ions (Na^+, Cl^-, Mg^{2+}, K^+, Ca^{2+}) reported in Figure 4 range from 0.05 to 0.5 μg m^{-3} in BGC to BGM, from 0.15 to 0.35 μg m^{-3} in ANTC to ANTM, and is close to 0.7 μg m^{-3} in EV. Sodium and chloride dominate the mass of these ions in BGM and ANTM (88 and 79%, respectively) and represent ~60% in BGC and ANTC. They are both located in a supermicron mode (Figure 5). Sodium levels at PDD are in general above those observed at Sonnblick that are most of time below 0.03 μg m^{-3} [*Kasper and Puxbaum*, 1998] and in the order of 0.01 to 0.1 μg m^{-3} in the mid troposphere at Mauna Loa [*Parrington and Zoller*, 1984]. In their study of precipitation at Col du Dôme (4250 m asl, French Alps) *Legrand et al.* [2002] pointed out the complexity to distinguish the fraction of sodium related to sea-salt and the one associated with dust in continental atmosphere, particularly in summer when calcium levels are 3 times higher than sodium ones. Considering samples in which sodium levels largely exceed calcium ones (BGM and ANTM, see Table 3) and for which we can assume a negligible impact of dust on sodium, we calculate a chloride loss of 20% in BGM and 67% in ANTM. This increase of chloride loss from BG to ANT is likely resulting from interaction between sea-salt and acidic species. Examination of the mass size distribution of chloride loss versus nitrate and sulfate (not shown) clearly indicates that nitric acid is the major specie causing the chloride volatilization. On a few ANT samples, chloride is shifted toward larger particles (>4 μm) while sodium and nitrate stay on sea-salt mode (1–3 μm). That suggests, among other possibilities, that HCl produced by interaction of sea-salt with nitric acid or by other nonmarine origin have condensed onto larger crustal particles, or that there is a more pronounced chloride loss for smaller sea salt particles than for larger (because the available surface is higher).

[40] The main fraction of potassium, magnesium and calcium present in supermicron range are of marine origin in BGM, as suggested the potassium, magnesium and calcium to sodium ratios (0.03, 0.2, and 0.035, respectively) close to seawater composition seen in sample 1 for instance. In other air masses, the non-sea-salt fraction of the three cations is significant, non-sea-salt calcium and magnesium levels varying from 0.08 (BGC) to 0.017 μg m^{-3} (ANT) and from 0.05 (BGC) to 0.010 μg m^{-3} (ANT), respectively. Being present in supermicron range generally centered at 5.8 μm GMD, the non-sea-salt fractions of calcium and magnesium are likely of crustal origins.

[41] The non-sea-salt potassium level varies from 0.03 to 0.016 μg m^{-3} in BGC and ANT, respectively. In contrast to calcium and magnesium, the non-sea-salt fraction of potassium is still present in submicron modes

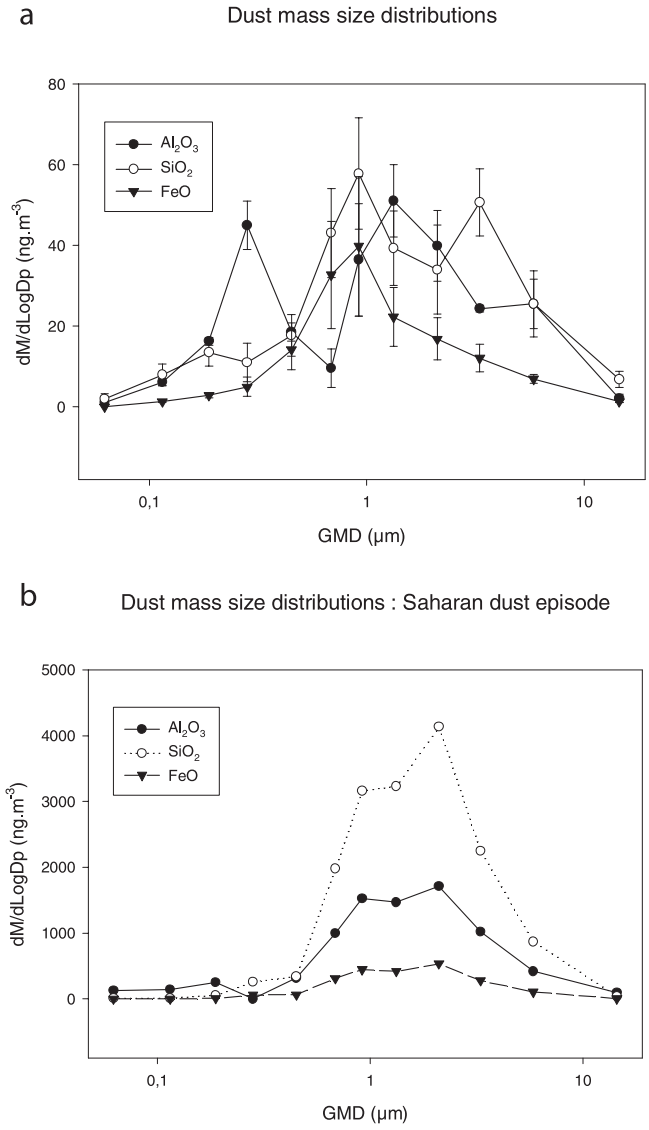

Figure 6. Dust mass size distributions for (a) all analyzed samples but sample 11 and (b) sample 11 (Saharan dust episode).

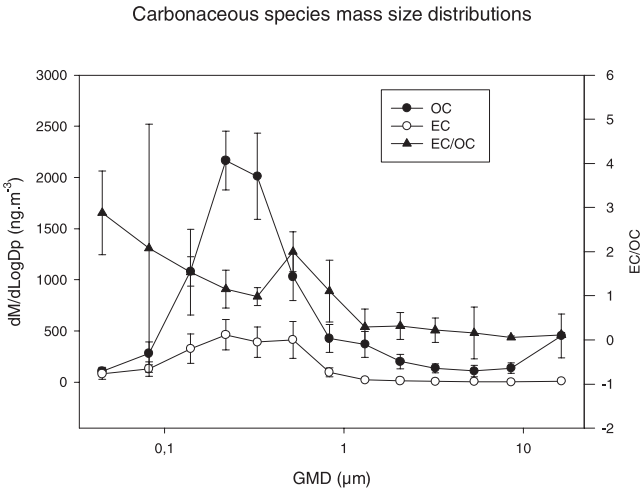

Figure 7. Mass distribution for carbonaceous species for all analyzed samples.

indicating the existence of a noncrustal and nonmarine source for this specie. The non-sea-salt fractions of calcium and magnesium are both two times higher in BGC than in ANT whereas the non-sea-salt potassium fraction is 5 times higher in ANT than in BGC, supporting the assumption of an anthropogenic source of potassium, and most probably biomass or biofuel combustion sources [*Andreae*, 1983; *Andreae et al.*, 1996; *Reiner et al.*, 2001]. Indeed, submicron K^+ is associated to the same sizes than OCBC rather than to the inorganic components, for samples 5, 7, 9 and 11 (winter 2000). Instead, submicron K^+ is associated to inorganic species rather than OC or BC for samples 14, 17, 19 and 20 (winter 2001). Stage to stage correlations are stronger between K_{sub} and BC than between K_{sub} and OC.

[42] The mass size distribution of dust reported in Figure 6a for all analyzed samples but sample 11. Submicron Al and Si is observed, rather located on the Acc1 mode than on the Acc2 mode; thus they may not be found as Al_2O_3 and SiO_2 in this size range. Several supermicron modes are necessary to describe the mineral distribution. FeO is located around 1 µm diameter particles while Al_2O_3 and SiO_2 have a common mode at 1.3 µm GMD; Al_2O_3 has another peak at 6 µm GMD while SiO_2 is at 3 µm. These differences may be due to a change of the densities of the mineral assemblages, but uncertainties on the mass size distributions are high considering the low concentrations usually found in the air masses encountered at the PDD. However, the campaign was characterized by a remarkable Saharan dust episode on 12 February (sample 11 in Table 3, denoted EVM). The yellow-brownish dust deposits on impaction substrates and the high mineral fraction (23% of the total mass) are uniquivocal evidences for a Saharan dust event. In contrast to what is commonly observed in PDD samples, the coarse mode is dominant (52%, Table 4). Mineral concentrations are 20 to 30 times higher than in other samples, major components being silicon, aluminum and sulfur. These outstanding concentrations have already been observed during another Saharan dust event at the Jungfraujoch [*Schwikowski et al.*, 1995]. The mass size distribution of this sample is characterized by 2 modes, all species except sulfur having a main mode located at 2 µm. Sulfur is on submicron particles (0.45 µm) along with a secondary mode for Mg, K, Na, Cl, and Zn. Significant stage to stage correlations are found for Si, Al and Fe with Si/Al and Fe/Al ratios of 2.21 and 0.5, respectively. These values are very close to the ratio of 2.03 and 0.39 measured at Jungfraujoch during a Saharan dust event [*Schwikowski et al.*, 1995]. According to *Bergametti et al.* [1989], such low values are found to be typical for Saharan dust particles with sources

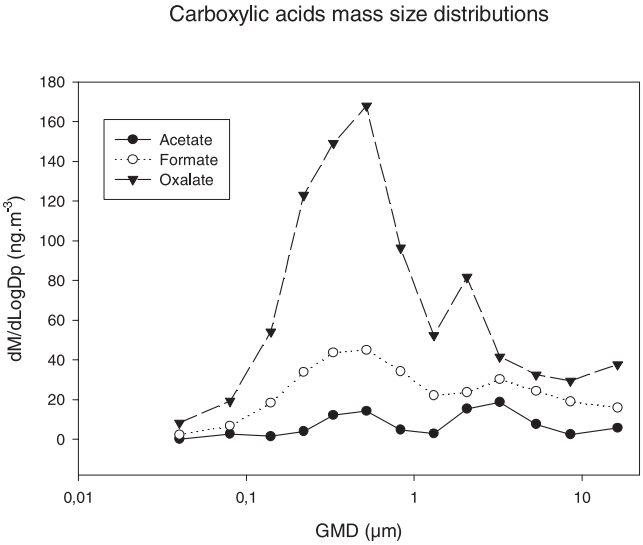

Figure 8. Organic acids mass size distributions for all analyzed samples.

Table 4. Mass Contributions of the Analyzed Species to Acc1, Acc2, and Coarse Modes for Each Type of Aerosol

	Percent Sum						
	Inorganic	ECOC-OA	OC-OA	EC	OA	Dust	ND
			BGM				
Acc1	23	74			3		
Acc2	68	28			4		
Coarse	76	20			4		
			BGC				
Acc1	26		53	6	1		14
Acc2	48		39	5	3		5
Coarse	20		57	1	5		17
			ANTM				
Acc1	67	28			2	3	
Acc2	77	17			3	3	
Coarse	80	12			3	5	
			ANTC				
Acc1	40		45	12	1	2	
Acc2	61		24	11	1	3	
Coarse	63		17	2	4	14	
			EVM				
Acc1	54	36			3	7	
Acc2	74	14			1	11	
Coarse	48	7			1	44	
			EVC				
Acc1	29		39	26	2		4
Acc2	63		16	10	2		9
Coarse	43		10	3	4		40

regions in Algeria, Tunisia, and Libya, compared to regions in Morocco, western Algeria, and further south. Note here that despite a very high mass loading EVC does not show large concentration of dust indicators such as Ca^{2+} and has a different origin than the Saharan region. This interesting event will be discussed in the next section.

6.2. Organic Species

[43] Total carbon (TC) levels calculated from the sum of all impactor stages are similar in 2000 and 2001 although the analytical method differs (section 2). 90% of concentrations range between 0.5 and 2.9 $\mu g\ m^{-3}$. Such levels are usually found in rural, marine or remote sites [*Chow et al.*, 1996; *Turpin et al.*, 1997] and are far lower than typical concentrations observed in urban areas where they often exceed 25 $\mu g\ m^{-3}$ [*Nunes and Pio*, 1993; *Chen et al.*, 1997]. The highest TC concentration is found in the EVC sample (8.1 $\mu g\ m^{-3}$). With 4.7, 4.0, and 1.5 $\mu g\ m^{-3}$ of sulfate, nitrate and ammonium, this sample also exhibits the highest load of inorganic ions suggesting a strong anthropogenic input.

[44] Except in the EVC, sample which contains 2.9 $\mu g\ m^{-3}$ of EC and 5.1 $\mu g\ m^{-3}$ of OC, OC and EC levels (only determined in 2001) range from 1.2 to 2.2 $\mu g\ m^{-3}$ and 0.11 to 0.72 $\mu g\ m^{-3}$, respectively. Winter concentrations of BC measured by aethalometer at the site are close to 0.2 $\mu g\ m^{-3}$. EC levels at PDD are therefore similar to those recently measured at Mount Rax (1205 m asl, Austria) (0.43 and 0.73 $\mu g.m^{-3}$ in 1999 and 2000 [*Hitzenberger et al.*, 2001] and higher than BC levels of 0.007–0.104 $\mu g\ m^{-3}$ found at Sonnblick [*Nyeki et al.*, 1998]. If confirmed such a difference would suggest a shorter atmospheric lifetime of BC with respect to inorganic species such as sulfate for which levels were comparable between PDD and Sonnblick (see section 6.1). Note however that at Sonnblick there is a significant level of SO_2 in February and March 1992–1992 (8.5 and 15 $nmol\ m^{-3}$ [*Kasper and Puxbaum*, 1998]).

[45] While some authors reported similar EC/OC ratio whatever the considered regions and seasons [*Novakov et al.*, 2000; *Offenberg and Baker*, 2000], PDD samples exhibits a large variability (from 0.06 to 0.56 with a mean value of 0.3). The mean PDD value is close to the averaged value of 0.22 reported at Mount Rax [*Fuzzi*, 2000]. The lowest value seen at PDD is close to the one measured at remote sites on fine aerosols (0.09) by *Turpin et al.* [1997] and at remote sites (0.03) by *Heintzenberg* [1989]. *Chen et al.* [1997] measured mean EC/OC ratios of 0.71 and 1.53 for urban and rural sites, respectively. At PDD, highest EC/OC ratios are found for heavily loaded samples corresponding to northeastern transport (samples 15 and 17, Table 3) belonging to EVC and ANTC classes. Conversely, the lowest ratio is seen in samples 13 and 20 (BGC) corresponding to western transport. These changes are mainly due to a decrease in EC from ANTC levels ($0.57 \pm 0.21\ \mu g\ m^{-3}$) to BGC levels ($0.12 \pm 0.01\ \mu g\ m^{-3}$) whereas similar OC levels are present ($\sim 1.7\ \mu g\ m^{-3}$) in the 2 types of air masses (Table 3). This would imply either a secondary production of organic aerosol during the transport, considerably higher compared to EC; either a higher wet deposition scavenging efficiency for EC compared to OC.

[46] On average, 80% of the total carbon is present below 0.5 μm (Figure 7). 90% of OC is smaller than 2 μm, predominantly present in Acc1 with sometimes a secondary mode at 1.3 μm GMD. This is in agreement with many studies indicating OC associated to the fine particle fraction [*Temesi et al.*, 2001; *Chen et al.*, 1997; *Nunes and Pio*, 1993] and for which a bimodal distribution was also reported by *Offenberg and Baker* [2000].

[47] The mass distribution of EC is also bimodal with a first mode similar to the OC one (at 0.2 μm, Acc1) and a second one at 0.5 μm (Acc2). The mass size distribution of EC at PDD therefore differs from that reported by *Offenberg and Baker* [2000] in over-water and rural samples showing a single mode centered between 0.45 and 1.4 μm GMD. A secondary mode is often found at larger particle sizes (>12 μm) in urban areas [*Offenberg and Baker*, 2000]. The presence of EC in the Acc2 mode suggests an internal mixing with inorganic species. In fact, EC of the Acc2 mode behaves, in cloud, in a similar way to the very soluble inorganic species [*Sellegri et al.*, 2003], which might be attributed to its alteration by inorganics.

[48] As EC and OC being not present in the same modes, their ratio is size dependent. The EC/OC ratio is maximum (0.4) at 0.5 μm GMD (Acc2) indicating internal mixing of EC with inorganic species and on very small particles (0.8) at 0.045 μm GMD (Figure 7). The EC/OC ratio is close to 0.25 between 0.1 and 0.3 μm, where most of the carbon mass is present. Supermicron particles show low EC/OC ratio (0.05). *Offenberg and Baker* [2000] found a constant ratio of 0.3 regardless of particle size, but their samples were separated into 2 classes only. *Chen et al.* [1997] found a marked bimodal size distribution of EC/OC with values of 0.8 at 0.06–0.32 μm and 1.1 at 0.32–1.8 μm.

[49] At PDD, oxalate is among identified organic acids present in the aerosol phase the most abundant species (55% of total), followed by formate (24%) and acetate (13%). This is in agreement with numerous studies that have found oxalate as the most abundant dicarboxylic acid present in aerosols from various regions (urban, marine, arctic as well as in the free troposphere [*Limbeck and Puxbaum*, 2000; *Baboukas et al.*, 2000; *Kawamura et al.*, 1996; *Kerminen et al.*, 1999]), others including succinate and glutarate [*Limbeck and Puxbaum*, 2000]. Oxalate levels are in the same order of magnitude than the sum of formate and acetate but these later were found to be far more abundant in the gas phase at PDD even during cloud events [*Voisin et al.*, 2000]. No correlation is found between bulk concentrations of major man-made derived species such as sulfate and nitrate and bulk concentrations of oxalate suggesting that natural sources dominate the present-day budget of this specie. Since the lowest value are found in BGM class, we propose that continental biogenic emissions as the main source for this specie. While oxalate is mostly submicronic, formate and acetate are clearly both submicronic and supermicronic (Figure 8). Although oxalate is not correlated to sulfate and ammonium when considering bulk concentrations, it is located on the same particle size than these species, indicating eventual gaseous condensation process during transport and subsequent internal mixing with inorganic species.

6.3. Organic/Inorganic Apportionment Versus Size

[50] On average, Acc1 and Acc2 modes account for 48% and 46% of the submicron mass (<1.3 μm), respectively. These contributions are variable depending on aerosol

origin, 54% and 36% respectively in BG, 43% and 48% in ANT, 30% and 59% in EVC. Background samples generally show predominant Acc1 mode whereas ANT and EV exhibit a predominant Acc2 mode. Overall, the mass fraction on the Acc2 mode tends to increase with increasing anthropogenic influence leading to increasing contribution of inorganic species. Moreover, the size distribution is shifted from small to larger particle sizes when going from background to highly loaded samples (Figures 3a and 3b).

[51] Inorganic and carbonaceous species account for 35% and 62%, respectively, of the total mass in Acc1, and 57% and 41%, respectively in Acc2. The proportion of carbon decreases with increasing particle size. The contributions of organic acids and insoluble mineral to the total aerosol mass never exceed 4% of the total analyzed compounds, except for the Saharan dust even in which the mineral contribution reaches 10% of the total mass.

[52] The belonging of carbonaceous species to a mode of smaller particles than inorganic species is contrary to the findings of *Temesi et al.* [2001], who found both ionic and carbonaceous species associated onto 0.5 μm GMD particle, with an additional nucleation mode at 0.04 μm for carbonaceous particles only. However, the trend of largest particles containing the smallest fraction of carbon, while smallest particles contain the greatest proportion has already been documented in the literature [*Offenberg and Baker*, 2000].

[53] Examination of Figures 4a to 4f shows that the mass fraction of TC increases with decreasing aerosol loading of samples. This feature is observed for both continental unimodal samples and marine bimodal samples. In each class, the mass fraction (and concentrations) of TC increases from marine bimodal samples to continental unimodal samples. Similar observations have been reported by *Putaud et al.* [2000] in the MBL with background samples containing 20% of OC and 30% of $nssSO_4$ whereas anthropogenic influenced samples contain 12% of OC and 58% of $nssSO_4$. *Novakov et al.* [1997] showed that the carbon mass fraction increases with altitude and the remoteness of the air masses, confirming therefore our observations. The source of carbon species is therefore clearly continental and its relative contribution increases with distance from anthropogenic sources. This can be explained by the longer residence time of carbonaceous particles compare to inorganic ions from lower scavenging efficiency [*Sellegri et al.*, 2003]. This observation cannot be applied to EC though since the decrease of EC by a factor of 5 between ANTC and BGC is larger than the decrease of sulfate (a factor of 2) implying an even shorter atmospheric lifetime for EC compared to sulfate.

[54] The higher concentrations of inorganic species, relative to carbonaceous species, in ANTC samples compared to BGC samples can also be due to the fact that anthropogenic sources presently emit relatively larger amounts of inorganic. Finally, condensation of biogenic VOCs onto Acc1 particles can also contribute to the observed behavior of carbon species.

7. Summary and Conclusions

[55] Three different kinds of aerosol population were found in the free troposphere at Puy de Dôme in winter/spring on the basis of their aerosol mass loading and composition: background, anthropogenic and special events.

[56] 1. BG samples are characterized by low NO_3^-, SO_4^{2-} concentrations (50–190 ng m^{-3} and 134–160 ng m^{-3}). Relatively high Na^+ concentrations (265–515 ng m^{-3}) are found associated with the presence of a sea-salt mode. In that case, the aerosol is either neutral or alkaline and loss of chlorine appears extremely limited. In the absence of a coarse mode, the aerosol is acidic and characterized by relatively higher OC content (1700 ng m^{-3}, i.e., 55% of total mass) externally mixed with inorganic species. This high carbonaceous fraction exhibits a low EC/OC ratio (0.07) suggesting, either formation of OC from organic gaseous precursors, condensing onto organic particles as indicated by the very limited degree of internal mixing with inorganic ions, either a preferential wet deposition scavenging efficiency of EC compared to OC.

[57] 2. ANT samples are the most frequent aerosol type at the Puy de Dôme. They are characterized by an abundance of inorganic fraction in the submicron range. This high fraction is mainly composed of sulfate (450–1100 ng m^{-3}), nitrate and ammonium (420–900 ng m^{-3} and 75–500 ng m^{-3}, respectively). However, nitrate in ANT samples is showing the highest raise to BG samples (by a factor 3.8), compared to sulfate (factor 3.2) and ammonium (factor 2.9). Consequently, nitrate is the main inorganic component responsible for the acidification of the aerosol in anthropogenic air masses. Overcome of nitrate over sulfate in the acidification of aerosols has already been observed over Europe [*Schaap et al.*, 2002, and reference therein], and might indicate an evolution in the pollution sources. The mass fraction of OC is rather low (25 and 42% for marine and continental classes) and the concentrations (660–2250 ng m^{-3}) are equivalent to those found in BG, mostly found on the first accumulation mode (Acc1). Here again, this might indicate lower scavenging efficiency of OC compared to inorganic species during transport from ANT to BG. When present Na^+ concentration are similar to those found in BG (260–560 ng m^{-3}) but an important depletion of chloride is observed with respect to sea-salt, chloride being often substituted by nitrate. While the OC fraction is decreasing, EC fraction is increasing from BG to ANT, and also shows higher degree of mixing with inorganic ions.

[58] 3. The Saharan dust event shows the highest proportion of dust as well as $nssCa^{2+}$ and $nssK^+$ and lowest proportion of organic carbon. It also contains high concentrations of nitrate indicating that mineral dust provides an ideal surface for gases to condense. The EVC sample is highly suspected to be representative of a boundary layer input into the free troposphere. Overall, highly loaded samples (Saharan dust event (EVM) and boundary layer intrusion (EVC)), exhibit the highest nitrate fraction. Nitrate levels are 7.5 times higher than in ANTC samples (to be compared to an increase of 3.8 for both sulfate and ammonium between ANT and EV), confirming the high level of nitrate contamination with the anthropogenic influence.

[59] External mixing between inorganic and organic carbon is an important feature of the aerosol sampled at the

Puy de Dôme, whatever the air mass type, with important consequences on the scavenging properties of this aerosol.

[60] **Acknowledgments.** This work was supported by CNRS-INSU under the National Program for Atmospheric Research (PNCA) and by the Ministère de la Recherche under ACI-Jeune Chercheur to PL. Authors acknowledge financial support from the scientific council of region Auvergne and from Observatoire de Physique du globe de Clermont-Ferrand (OPGC).

References

Andreae, M. O., Soot carbon and excess fine potassium: Long-range transport of combustion-derived aerosols, *Science*, *220*, 1148–1151, 1983.

Andreae, M. O., E. Atlas, H. Cachier, W. R. Cofer, G. W. Harris, G. Helas, R. Koppmann, J.-P. Lacaux, and D. E. Ward, Trace gas and aerosol emissions from savanna fires, in *Biomass Burning and Global Change*, edited by J. S. Levine, pp. 278–295, MIT Press, Cambridge, Mass., 1996.

Baboukas, E. D., M. Kanakidou, and N. Mihalopoulos, Carboxylic acids in gas and particulate phase above the Atlantic Ocean, *J. Geophys. Res.*, *105*, 14,459–14,471, 2000.

Barth, M. C., P. J. Rasch, J. T. Kiehl, C. M. Benkovitz, and S. E. Schwartz, Sulfur chemistry in the National Center for Atmospheric Research community climate model: Description, evaluation, features, and sensitivity to aqueous chemistry, *J. Geophys. Res.*, *105*, 1387–1415, 2000.

Bergametti, G., L. Gomes, E. Remoudaki, M. Desbois, D. Martin, and P. Buat-Ménard, Present transport an deposition patterns of African dust to the north-western Mediterranean, in *Paleoclimatology and Paleometeorology: Modern and Past Patterns of Global Atmospheric Transport*, edited by M. Leinen and M. Sarthein, pp. 227–252, Kluwer Acad., Norwell, Mass., 1989.

Buseck, P. R., and M. Posfai, Airborne minerals and related aerosol particles: Effect on climate and environment, *Proc. Natl. Acad. Sci. U.S.A.*, *96*, 3372–3379, 1999.

Cachier, H., M. P. Brémond, and P. Buat-Ménard, Determination of atmospheric soot carbon with a simple thermal method, *Tellus, Ser. B*, *41*, 379–390, 1989.

Chen, S.-J., S.-H. Liao, W.-J. Jian, and C.-C. Lin, Particle size distribution of aerosol carbon in ambient air, *Environ. Int.*, *23*(4), 475–488, 1997.

Chow, J. C., J. G. Watson, L. C. Pritchett, W. R. Pierson, C. A. Frazier, and R. G. Purcell, The DRI Thermal/Optical Reflectance Carbon Analysis System: Description, evaluation and applications in U.S. air quality studies, *Atmos. Environ., Part A*, *27*(8), 1185–1201, 1993.

Chow, J., A. J. Watson, Z. Lu, D. H. Lowenthal, C. A. Frazier, A. M. Solomon, R. H. Thuillier, and K. Magliano, Descriptive analysis of PM2. 5 and PM10 at regionally representative locations during SJVAQS/AUSPEX, *Atmos. Environ.*, *30*, 2079–2112, 1996.

Clarke, A. D., J. N. Porter, F. P. J. Valero, and P. Pilewskie, Vertical profiles, aerosol microphysics, and optical closure during the Atlantic Stratocumulus Transition Experiment: Measured and modelled column optical properties, *J. Geophys. Res.*, *101*, 4443–4453, 1996.

Fuzzi, S., PROCLOUD annual report, 57 pp., EUROTRAC-2, Munich, Germany, 2000.

Hämeri, K., et al., Hygroscopic growth of the ultrafine ammonium sulfate aerosol measured using an ultrafine tandem differential mobility analyzer, *J. Geophys. Res.*, *105*, 22,231–22,242, 2000.

Hansson, H.-C., M. J. Rood, S. Koloutsou-Vakakis, K. Hämeri, D. Orsini, and A. Wiedensohler, NaCl aerosol particle hygroscopicity dependence on mixing with organic compounds, *J. Atmos. Chem.*, *31*, 321–346, 1998.

Heintzenberg, J., Fine particles in the global troposphere: A review, *Tellus, Ser. B*, *41*, 149–160, 1989.

Heintzenberg, J., and D. S. Covert, On the distribution of physical and chemical particle properties in the atmospheric aerosol, *J. Atmos. Chem.*, *10*, 383–397, 1990.

Hinds, W. C., *Aerosol Technology: Properties, Behavior, and Measurement of Airborne Particles*, 2nd ed., John Wiley, New York, 1998.

Hitzenberger, R., A. Berner, R. Kromp, A. Kasper-Giebl, A. Limbeck, W. Tscherwenka, and H. Puxbaum, Black carbon and other species at a high-elevation European site (Mount Sonnblick, 3106 m, Austria): Concentrations and scavenging efficiencies, *J. Geophys. Res.*, *105*, 24,637–24,645, 2000.

Hitzenberger, R., A. Berner, H. Giebl, K. Drobesch, A. Kasper-Giebl, M. Loeflund, H. Urban, and H. Puxbaum, Black carbon (BC) in alpine aerosols and cloud water-concentrations and scavenging efficiencies, *Atmos. Environ.*, *35*, 5135–5141, 2001.

Howell, S., A. Pszenny, P. K. Quinn, and B. J. Huebert, A field comparison of three cascade impactors, *Aerosol Sci. Technol.*, *29*, 475–492, 1999.

Huebert, B. J., L. Zhuang, S. Howell, K. Noone, and B. Noone, Sulfate, nitrate, methanesulfonate, chloride, ammonium, and sodium measurements from ship, island, and aircraft during the Atlantic Stratocumulus Transition Experiment/Marine Aerosol Gas Exchange, *J. Geophys. Res.*, *101*, 4413–4423, 1996.

Intergovernmental Panel on Climate Change (IPCC), *Climate Change 2001: The Scientific Basis*, edited by J. T. Houghton et al., Cambridge Univ. Press, New York, 2001.

Jacobson, M. C., H.-C. Hansson, B. Noone, and R. J. Charlson, Organic atmospheric aerosols: Review and state of the science, *Rev. Geophys.*, *38*(2), 267–294, 2000.

Jennings, S. G., et al., Microphysical and physico-chemical characterization of atmospheric marine and continental aerosol at Mace Head, *J. Aerosol Sci.*, *31*(17), 2795–2808, 1997.

Kasper, A., and H. Puxbaum, Seasonal variation of SO_2, HNO_3, NH_3, and selected aerosol components at Sonnblick (3106 m a. s. l.), *Atmos. Environ.*, *32*, 3925–3939, 1998.

Kawamura, K., H. Kasukabe, and L. Barrie, Source and reaction pathways of dicarboxylic acids, ketoacids, and dicarbonyls in arctic aerosols: One year of observations, *Atmos. Environ.*, *30*, 1702–1722, 1996.

Kerminen, V., and A. S. Wexler, Growth laws of atmospheric aerosol particles: An examination of the bimodality of the accumulation mode, *Atmos. Environ.*, *22*, 3263–3275, 1995.

Kerminen, V., K. Teinilä, R. Hillamo, and J. Makela, Size-segregated chemistry of particulate dicarboxylic acids in the arctic atmosphere, *Atmos. Environ.*, *33*, 2089–2100, 1999.

Krivacsy, Z., et al., Study on the chemical character of water soluble organic compounds in fine atmospheric aerosol at the Jungfraujoch, *J. Atmos. Chem.*, *39*, 235–259, 2001.

Lavanchy, V. M. H., H. W. Gäggeler, S. Nyeki, and U. Baltensperger, Elemental carbon (EC) and black carbon (BC) measurements with a thermal method and an aethalometer at the high-alpine research station Jungfraujoch, *Atmos. Environ.*, *33*, 2759–2769, 1999.

Legrand, M., S. Preunkert, D. Wagenbach, and H. Fischer, Seasonally resolved Alpine and Greenland ice core records of anthropogenic HCl emissions over the 20th century, *J. Geophys. Res.*, *107*(D12), 4139, doi:10.1029/2001JD001165, 2002.

Lesins, A., P. Chylek, and U. Lohmann, A study of internal and external mixing scenarios and its effect on aerosol optical properties, *J. Geophys. Res.*, *107*(D10), 4094, doi:10.1029/2001JD000973, 2002.

Limbeck, A., and H. Puxbaum, Dependence of in-cloud scavenging of polar organic aerosol compounds on the water solubility, *J. Geophys. Res.*, *105*, 19,857–19,867, 2000.

Maenhaut, W., R. Hillamo, J. M. Mäkelä, J.-L. Jaffrezo, M. H. Bergin, and C. I. Davidson, A new cascade impactor for aerosol sampling with subsequent PIXE analysis, *Nucl. Instrum. Methods Phys. Res., Sect. B*, *109/110*, 482–487, 1996.

Maupetit, F., and R. Delmas, Snow chemistry of high altitude glaciers in the French Alps, *Tellus, Ser. B*, *46*, 304–324, 1994.

McDow, S. R., and J. J. Hnutzicker, Vapor adsorption artifact in the sampling of organic aerosol: Face velocity effects, *Atmos. Environ., Part A*, *24*, 2563–2571, 1990.

Meng, Z., and J. G. Seinfeld, On the source of submicrometer droplet mode of urban and regional aerosols, *Aerosol Sci. Technol.*, *20*, 253–265, 1994.

Neusüß, C., D. Weise, W. Birmili, H. Wex, A. Wiedensholer, and D. S. Covert, Size-segregated chemical, gravimetric and number distribution-derived mass closure of the aerosol in Sagres, Portugal during ACE-2, *Tellus, Ser. B*, *52*, 169–184, 2000.

Novakov, T., D. A. Hegg, and P. V. Hobbs, Airborne measurements of carbonaceous aerosols on the East Coast of the United States, *J. Geophys. Res.*, *102*, 30,023–30,030, 1997.

Novakov, T., et al., Shipboard measurements of concentrations and properties of carbonaceous aerosols during ACE-2, *Tellus, Ser. B*, *52*, 228–238, 2000.

Nunes, T. V., and C. A. Pio, Carbonaceous aerosols in industrial and coastal atmospheres, *Atmos. Environ., Part A*, *27*, 1339–1346, 1993.

Nyeki, S., U. Baltensperger, I. Colbeck, D. T. Jost, E. Weingartner, and H. W. Gäggeler, The Jungfraujoch high-alpine research station (3454 m) as a background clean continental site for the measurement of aerosol parameters, *J. Geophys. Res.*, *103*, 6097–6107, 1998.

Offenberg, J. H., and J. E. Baker, Aerosol size distribution of elemental and organic carbon in urban and over-water atmospheres, *Atmos. Environ.*, *34*, 1509–1517, 2000.

Parrington, J. R., and W. H. Zoller, Diurnal and long term temporal changes in the composition of atmospheric particles at Mauna Loa, Hawaii, *J. Geophys. Res.*, *89*, 2522–2534, 1984.

Posfai, M., J. R. Xu, J. Anderson, and P. R. Buseck, Wet and dry sizes of atmospheric aerosol particles: An AFM-TEM study, *Geophys. Res. Lett.*, *25*, 1907–1910, 1998.

Preunkert, S., M. Legrand, D. Wagenbach, and H. Fischer, Sulfate trends in a Col du Dôme (French Alps) ice core: A record of anthropogenic sulfate levels in the European midtroposphere over the twentieth century, *J. Geophys. Res.*, *106*, 31,991–32,004, 2001.

Putaud, J. P., et al., Chemical mass closure and assessment of the origin of the submicron aerosol in the marine boundary layer and the free troposphere at Tenerife during ACE2, *Tellus, Ser. B*, *52*, 141–168, 2000.

Reiner, T., D. Sprung, C. Jost, R. Gabriel, O. L. Mayol-Bracero, M. O. Andreae, T. L. Campost, and R. E. Shetter, Chemical characterization of pollution layers over the tropical Indian Ocean: Signatures of emissions from biomass and fossil fuel burning, *J. Geophys. Res.*, *106*, 28,497–28,510, 2001.

Ricard, V., J.-L. Jaffrezo, V. Kerminen, R. Hillamo, M. Sillanpaa, S. Ruellan, C. Liousse, and H. Cachier, Two years of continuous aerosol measurements in northern Finland, *J. Geophys. Res.*, *107*(D11), doi:10.1029/2001JD000952, 2002.

Saxena, P., and L. M. Hildemann, Water-soluble organics in atmospheric particles: A critical review of the literature and application of thermodynamics to identify candidate compounds, *J. Atmos. Chem.*, *24*, 57–109, 1996.

Schaap, M., K. Müller, and H. ten Brink, Constructing the European aerosol nitrate concentration field from quality analyzed data, *Atmos. Environ.*, *36*, 1323–1335, 2002.

Schwikowski, M., P. Seibert, U. Baltensperger, and H. W. Gäggeler, A study of an outstanding Saharan dust event at the high-alpine site Jungfraujoch, Switzerland, *Atmos. Environ.*, *29*, 1829–1842, 1995.

Sellegri, K., J. Gourdeau, J.-P. Putaud, and S. Despiau, Chemical composition of marine aerosol in a Mediterranean coastal zone during the FETCH experiment, *J. Geophys. Res.*, *106*, 12,023–12,037, 2001.

Sellegri, K., P. Laj, R. Dupuy, M. Legrand, S. Preunkert, and J.-P. Putaud, Size-dependent scavenging efficiencies of multicomponent atmospheric aerosols in clouds, *J. Geophys. Res.*, *108*, doi:10.1029/2002JD002749, in press, 2003.

Temesi, D., A. Molnar, E. Meszaros, T. Feczko, A. Gelencser, G. Kiss, and Z. Krivacsy, Size resolved chemical mass balance of aerosol particles over rural Hungary, *Atmos. Environ.*, *35*, 4347–4355, 2001.

Turpin, B. J., and H. J. Lim, Species contributions to PM2.5 mass concentrations: Revisiting common assumptions for estimating organic mass, *Aerosol. Sci Technol.*, *35*, 602–610, 2001.

Turpin, B. J., J. J. Huntzicker, and S. V. Hering, Investigation of organic aerosol sampling artifacts in the Los Angeles basin, *Atmos. Environ.*, *28*, 3061–3071, 1994.

Turpin, B. J., P. Saxena, G. Allen, P. Koutrakis, P. McMurry, and L. Hildemann, Characterization of the Southwestern Desert aerosol, Meadview, AZ, *J. Air Waste Manage. Assoc.*, *47*, 344–356, 1997.

Viidanoja, J., V. Kerminen, and R. Hillamo, Measuring the size distribution of atmospheric organic and black carbon using impactor sampling coupled with thermal carbon analysis: Method development and uncertainties, *Aerosol. Sci. Technol.*, *36*, 607–616, 2002.

Voisin, D., M. Legrand, and N. Chaumerliac, Scavenging of acidic gases (HCOOH, CH_3COOH, HNO_3, HCl, and SO_2) and ammonia in mixed liquid-solid water clouds at the Puy de Dôme mountain, *J. Geophys. Res.*, *105*, 6817–6836, 2000.

Wagenbach, D., S. Preunkert, J. Schaefer, W. Jung, and L. Tomadin, Northward transport of Saharan dust recorded in a deep Alpine ice core, in *The Impact of African Dust Across the Mediterranean*, edited by S. Guerzoni and R. Chester, pp. 291–300, Kluwer Acad., Norwell, Mass., 1996.

Warneck, P., *Chemistry of the Natural Atmosphere*, 2nd ed., 927 pp., Academic, San Diego, Calif., 2000.

Weast, R. C., *Handbook of Chemistry and Physics*, CRC Press, Boca Raton, Fla., 1984.

Zappoli, S., et al., Inorganic, organic and macromolecular components of fine aerosol in different areas of Europe in relation to their water solubility, *Atmos. Environ.*, *33*, 2733–2743, 1999.

H. Cachier, Laboratoire des Sciences du Climat et de l'Environnement, CNRS, Bat. 12, Avenue de la Terrasse, F-91198 Gif sur Yvette Cedex, France.

R. Dupuy, P. Laj, F. Peron, and K. Sellegri, Laboratoire de Météorologie Physique, CNRS, Université Blaise Pascal, OPGC/CNRS, 24 avenue des Landais, F-63177 Aubière Cedex, France.

G. Ghermandi, Dipartimento di Ingegneria Meccanica e Civile, Università di Modena e Reggio Emilia, Via Vignolese 905, I-41100 Modena, Italy.

M. Legrand and S. Preunkert, Laboratoire de Glaciologie et Géophysique de l'Environnement, 54 rue Molière, F-38402 St. Martin d'Hères Cedex, France.

J.-P. Putaud, Joint Research Center, TP 460, I-21020 Ispra (VA), Italy.